galaxies

MDPI

Article

LAMOST Spectroscopy and Gaia Photo-Astrometry for an Interstellar Extinction Study

Oleg Malkov *, Aleksandra Avdeeva and Dana Kovaleva

Institute of Astronomy of RAS, Moscow 119017, Russia; volosatykh.as14@physics.msu.ru (A.A.); dana@inasan.ru (D.K.)

* Correspondence: malkov@inasan.ru; Tel.: +7-495-951-7993

Abstract: The aim of this work is to establish the present accuracy and convergence of available estimates of galactic extinction. We determine the galactic interstellar extinction in selected high-latitude areas of the sky based on Gaia DR3 astrometry and photometry and spectroscopic data from the LAMOST survey. For this purpose, we choose 42 northern high-latitude sky areas surrounding supernovae that allowed establishing the accelerated expansion of the universe. We compare our results with the estimates accepted in that paper and find that they agree well, within observational errors. Simultaneously, the estimates for galactic extinction by other authors along the same sightlines show systematic differences, which can cause the distance to the extragalactic object to change by ±3–5%.

Keywords: interstellar extinction; surveys

1. Introduction

Dust produced by the nuclear burning of stars scatters and absorbs light according to the dust-reddening law. Consequently, mapping the dust is one of the central problems in astronomy. In previous works, various models have been proposed to describe interstellar extinction. The first one, developed by [1], considers a barometric (exponential) function:

$$A_V(b,d) = \frac{a_0 \cdot \beta}{sin|b|} \cdot \left(1 - exp\left(\frac{-d \cdot sin|b|}{\beta}\right)\right). \quad (1)$$

It represents the classical model of a homogeneous, semi-infinite absorbing layer with a density exponentially distributed with height. Here b and d are galactic latitude and distance from the observer to the star. The parameter β is the scale height, and a_0 is the extinction per unit length in the Galactic plane. In the original model [1], a_0 and β were constants; however, in subsequent publications, they are treated as functions of galactic coordinates (l, b) or galactocentric coordinates (r, ϕ, z). Other models have been proposed in the works of [2–7] (hereafter G23). In addition, 3D maps of dust distribution in the galaxy have been developed and published by various authors: [8–12].

LAMOST stellar spectra can be used to independently test the reddening. Stellar spectra are a sensitive test of the reddening because the broadband photometry of a star is almost entirely determined by three parameters: gravity, metallicity, and effective temperature. These atmospheric parameters can be determined using only the line information in the spectra, allowing the intrinsic broadband colors of the star to be predicted independently of the observed colors of the star. However, dust between the observer and the star will bias the observed colors relative to the intrinsic colors. The difference between the predicted intrinsic and measured colors is a measurement of the reddening of the star.

The cosecant (barometric) law (1) was used in our previous work [13] to describe the variation of the interstellar extinction in the radial direction, like most of the models mentioned above, but the variations on the sphere were described using harmonic functions. In

check for updates

Citation: Malkov, O.; Avdeeva, A.; Kovaleva, D. LAMOST Spectroscopy and Gaia Photo-Astrometry for an Interstellar Extinction Study. *Galaxies* **2024**, *12*, 65. https://doi.org/10.3390/galaxies12050065

Academic Editor: Fan Liu

Received: 31 July 2024
Revised: 19 September 2024
Accepted: 10 October 2024
Published: 17 October 2024

that work, we used Gaia EDR3 photometry [14] and spectroscopic parameters from LAMOST data [15,16]. Since LAMOST data only cover the Northern Celestial Hemisphere [13], lacks approximation points in the Southern sky, which reduces the reliability of the model in this region. In [17], we used the RAVE DR6 [18] data, which cover the southern sky, to conduct similar studies and improve the [13] model. We calculated the visual extinction in different high-latitude regions of the southern sky based on the temperatures of stars from RAVE DR6 and Gaia EDR3 photometry and astrometry [14]. We then estimated the parameters a_0 and β from Equation (1) for each of the selected regions. We approximated the parameters estimated in [17] together with those found in [13] using spherical harmonics across the entire sky.

Special attention is paid in the literature to a parameter called total galactic visual extinction, or galactic extinction, A_{gal}. It can be estimated from the galactic dust reddening for a sightline, assuming a standard extinction law. The reddening estimates were published by [19] who based their results on HI and galaxy counts, by [20] (hereafter SFD98), who combined results of IRAS and COBE/DIRBE, while [21] (hereafter SF11) provide new estimates of galactic dust extinction from an analysis of the Sloan Digital Sky Survey. A_{gal} plays an important role in the construction of the extragalactic distance scale, as it provides us with the extinction of extragalactic objects to make proper allowance for the dimming of the primary distance indicators in external galaxies by interstellar dust in our own galaxy. Galactic extinction can be derived from (1) under the assumption that $d \to \infty$:

$$A_{gal}(b) = \frac{a_0 \beta}{\sin|b|}. \quad (2)$$

The main goal of the present study is the development of software for the approximation of A_V(d)-relations for various areas in the sky, and its application to a set of selected areas. We assume that (1) satisfactorily reproduces the observed V-band interstellar extinction A_V for high galactic latitudes. Besides the a_0, β parameters, A_{gal} values (2) are determined for each area and compared with values published in the literature. Obviously, getting total extinction A_{gal} we are forced to ignore any inhomogeneities beyond the distance of the Gaia stars, such as the high latitude cirrus.

The paper is organized as follows: In Section 2, we describe the data that were used and calculate the visual extinction of objects at individual areas of the sky. In Section 3, we present the results of calculations and compare them with other publications. Finally, in Section 4, we draw our conclusions.

2. Data and Method

2.1. Observational Data

The present study used the stars contained in LAMOST DR5 [16] and Gaia DR3 [22] surveys for which the distances from Bailer-Jones catalogue [23] are presented. We selected all objects from LAMOST DR5 in 42 regions, each with a radius of 1.5 degrees, centered on the positions of 42 SNe Ia listed in Table 1 of [24]. These selected regions are plotted in Figure 1. We applied quality cuts to the LAMOST data by imposing SNRR > 30 AND SNRG > 30 conditions on the signal-to-noise ratio in the r and g bands accordingly. Next, we cross-matched the Gaia DR3 catalog using the XMatch service from CDS, with a matching radius of 1 arcsecond. Figure 2 shows the distribution of angular distances between matched objects, where the identification peak is observed at 0.1 arcseconds. The distances corresponding to the objects we selected from Gaia DR3 were obtained from [23].

The visual extinction A_V for each star has been computed using the following relation:

$$A_V = c_1/c_2 \times [(BP - RP)_0 - (BP - RP)]. \quad (3)$$

Here $c_2 \equiv A_G/A_V$, where A_G is the interstellar extinction in the Gaia G-band. Bono et al. [25] give 0.840 for c_2. We use the mean value of $c_1 \equiv A_G/E_{BP-RP}$ equal

to 2.02. This value is calculated for a G2V star using the extinction curve by [26] with $R_V \equiv A_V/E_{B-V} = 3.1$. Passband characteristics were taken from [27].

Only MS-stars with Gaia (BP, RP) photometry were used for the analysis. Luminosity class was estimated from LAMOST atmospheric parameters: only stars with a gravity value of $\log g \geq 4$ were selected. Intrinsic color index $(BP - RP)_0$ for MS-stars was estimated from $T_{\rm eff}$(LAMOST) with Mamajek's relations http://www.pas.rochester.edu/~emamajek/EEM_dwarf_UBVIJHK_colors_Teff.txt (accessed on 16 October 2024), see also [28].

To mitigate potential inaccuracies in the following results, whether arising from distance errors or biases in photometry and spectroscopy, we conducted a consistency check. We calculated the absolute magnitudes of the stars using the reddening estimated in (3) and distances from [23]. We then compared these calculated absolute magnitudes with the values predicted by [28] for the corresponding effective temperatures. Objects showing a discrepancy greater than 0.1 mag were excluded from further analysis. As a result of this procedure, one of the 42 areas (SN 1997F) did not contain a sufficient number of stars, and we excluded this area from further study. Other areas each contain 22 to 284 stars with known d and A_V values, altogether 4960 stars.

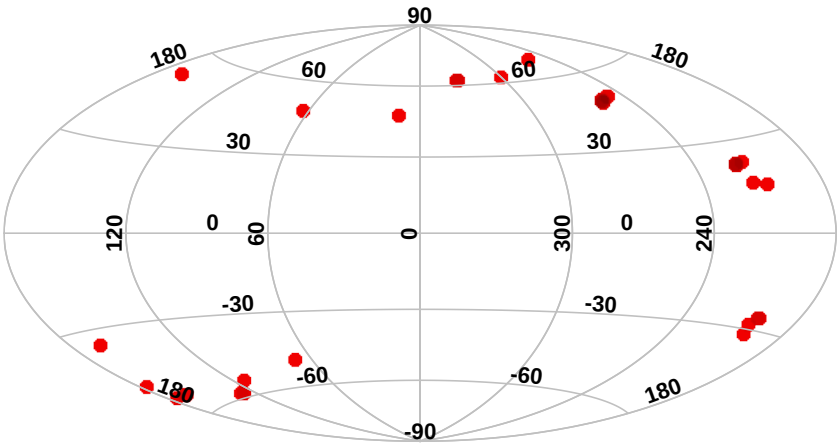

Figure 1. Selected areas. Galactic coordinates, Aitoff projection.

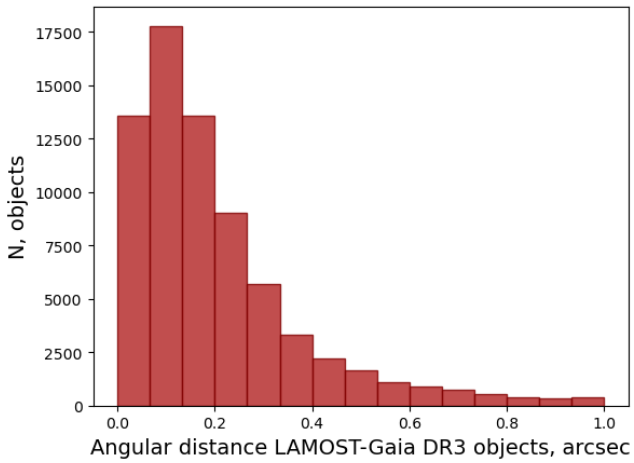

Figure 2. Angular distance between Gaia DR3 and LAMOST objects in the selected areas.

2.2. Estimation of Total Galactic Extinction

The process for obtaining the a_0 and β parameters is thoroughly explained in [13]. Here, we provide a brief overview, along with the modifications made for this specific task. The parameters were derived by minimizing the difference between the set of (d, A_V) values in each region and the function described in (1). The minimization was performed using the lmfit Python package [29]. An example of the results of a_0 and β determination

for three selected regions is shown in Figure 3; the red line if the function (1) calculated with obtained a_0 and β. We are primarily interested in the result at large distances, so we can ignore some discrepancy for nearby stars.

As noted in [13], degeneracy often arises during the calculation of a_0 and β. However, A_{gal} is typically well-defined and not subject to such degeneracy. For the purposes of this study, we derived A_{gal} and β instead of a_0 and β, which allows for a more accurate determination of the total Galactic extinction. The results of the approximation are presented in Table 1.

Table 1. Galactic extinction.

No	SN	l	b	N	A_{gal}	σA_{gal}	A_X	SFD98	SF11	E_{B-V}	G23
1	1992bi	63.26	47.24	76	0.054	0.007	0.03	0.032	0.027	0.019	0.182
2	1994F	258.61	68.13	65	0.070	0.014	0.11	0.118	0.094	0.022	0.150
3	1994G	162.89	52.78	89	0.044	0.080	0.03	0.026	0.022	0.02	0.116
4	1994H	173.06	−1.52	22	0.116	0.018	0.1	0.104	0.087	0.025	0.082
5	1994al	163.16	−1.82	27	0.427	0.024	0.42	0.449	0.369	0.132	0.526
6	1994am	173.10	−1.56	23	0.107	0.015	0.1	0.101	0.084	0.025	0.108
7	1994an	69.41	−1.08	115	0.245	0.010	0.21	0.218	0.18	0.055	0.300
8	1995aq	113.34	−1.60	34	0.134	0.012	0.07	0.072	0.059	0.029	0.247
9	1995ar	127.66	−1.47	166	0.108	0.005	0.07	0.071	0.059	0.028	0.131
10	1995as	127.76	−1.34	162	0.116	0.005	0.07	0.068	0.057	0.028	0.123
11	1995at	129.27	−1.14	145	0.107	0.005	0.07	0.063	0.053	0.028	0.213
12	1995aw	165.47	−1.08	284	0.098	0.004	0.12	0.132	0.11	0.03	0.186
13	1995ax	166.06	−1.91	278	0.090	0.080	0.11	0.11	0.091	0.029	0.158
14	1995ay	176.87	−1.45	116	0.270	0.012	0.35	0.378	0.31	0.047	0.428
15	1995az	202.11	−1.50	44	0.295	0.082	0.61	0.6	0.521	0.034	0.532
16	1995ba	215.99	22.98	273	0.100	0.007	0.06	0.059	0.048	0.024	0.110
17	1996cf	250.45	50.01	135	0.101	0.008	0.13	0.133	0.111	0.027	0.173
18	1996cg	220.77	22.15	148	0.111	0.019	0.11	0.116	0.096	0.027	0.181
19	1996ci	333.11	62.08	88	0.065	0.007	0.09	0.091	0.075	0.027	0.149
20	1996ck	301.41	62.10	33	0.059	0.011	0.13	0.106	0.088	0.022	0.224
21	1996cl	256.57	48.67	157	0.095	0.008	0.18	0.118	0.097	0.028	0.123
22	1996cm	10.89	46.74	107	0.120	0.009	0.15	0.155	0.127	0.031	0.236
23	1996cn	334.31	61.81	91	0.073	0.080	0.08	0.084	0.069	0.027	0.170
24	1997F	204.47	−1.45	1			0.13	0.133	0.112	0.037	0.234
25	1997G	202.33	−1.51	35	0.176	0.022	0.2	0.143	0.116	0.039	0.214
26	1997H	202.37	−1.21	31	0.200	0.029	0.16	0.169	0.138	0.04	0.220
27	1997I	202.37	−1.21	31	0.200	0.029	0.16	0.17	0.138	0.04	0.220
28	1997J	209.92	15.37	84	0.116	0.010	0.13	0.128	0.105	0.034	0.165
29	1997K	216.35	16.08	163	0.091	0.005	0.07	0.068	0.058	0.032	0.125
30	1997L	220.03	21.88	172	0.078	0.017	0.08	0.082	0.07	0.026	0.141
31	1997N	220.66	22.10	153	0.096	0.022	0.1	0.102	0.087	0.027	0.171
32	1997O	220.07	22.45	172	0.108	0.013	0.09	0.095	0.08	0.026	0.139
33	1997P	256.58	48.25	137	0.089	0.080	0.1	0.111	0.091	0.028	0.191
34	1997Q	256.88	48.38	139	0.093	0.008	0.09	0.099	0.081	0.028	0.168
35	1997R	256.95	48.50	142	0.094	0.009	0.11	0.099	0.08	0.028	0.140
36	1997S	256.96	48.70	146	0.092	0.008	0.11	0.109	0.089	0.028	0.178
37	1997ac	220.01	22.49	171	0.111	0.014	0.09	0.091	0.077	0.026	0.139
38	1997af	220.03	22.42	169	0.112	0.015	0.09	0.094	0.078	0.026	0.112
39	1997ai	249.96	50.36	141	0.107	0.007	0.14	0.15	0.123	0.027	0.133
40	1997aj	256.60	48.22	133	0.086	0.080	0.11	0.11	0.089	0.028	0.164
41	1997am	256.34	49.06	168	0.097	0.008	0.11	0.119	0.098	0.028	0.167
42	1997ap	333.65	61.90	95	0.071	0.006	0.13	0.087	0.071	0.027	0.105

Content of the table: SN designation, galactic coordinates, number of stars in the area (N), galactic extinction in mag: A_{gal} with uncertainty, A_X [24], A_V(SFD98) [20], A_V(SF11) [21], reddening E_{B-V} [9], A_V(G23) [7].

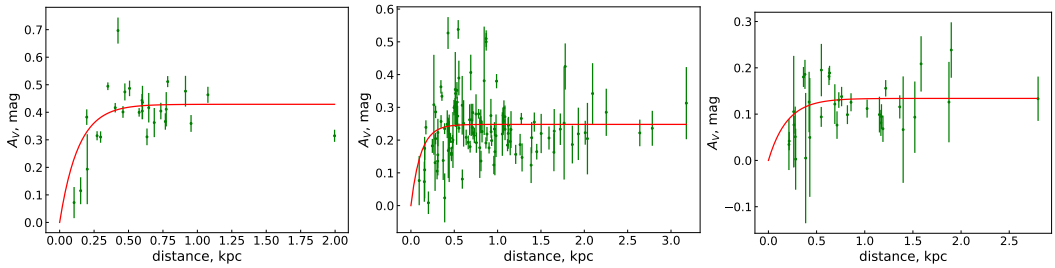

Figure 3. Examples of approximation of $A_V(d)$ dependence (red curves) in areas l,b = 163,−1 (**left**), l,b = 69,−1 (**middle**), and l,b = 111,−1 (**right**). Green points are stars in the area, with observational errors.

2.3. Error Budget

For each area, we estimated the effect of temperature measurement error on A_{gal} as follows. The effective temperature value for the objects in each area was modified by adding Gaussian noise. Specifically, each area was assigned a set of 1000 datasets whose temperature distribution for each object is a normal distribution with a standard deviation σ equal to the temperature measurement error of that object in the LAMOST survey. For the 1000 datasets, we then calculated A_{gal} values, which we characterize by the median Q_2, as well as upper (Q_3) and lower (Q_1) quartiles.

In the vast majority of cases (see Figure 4), the distribution turned out to be quite symmetrical;

$$|(Q_3 - Q_2) - (Q_2 - Q_1)| < 0.^m002, \tag{4}$$

therefore, a value equal to half of the interquartile range IQR was used as dispersion in the following: IQR/2 = $(Q_3 - Q_1)/2$.

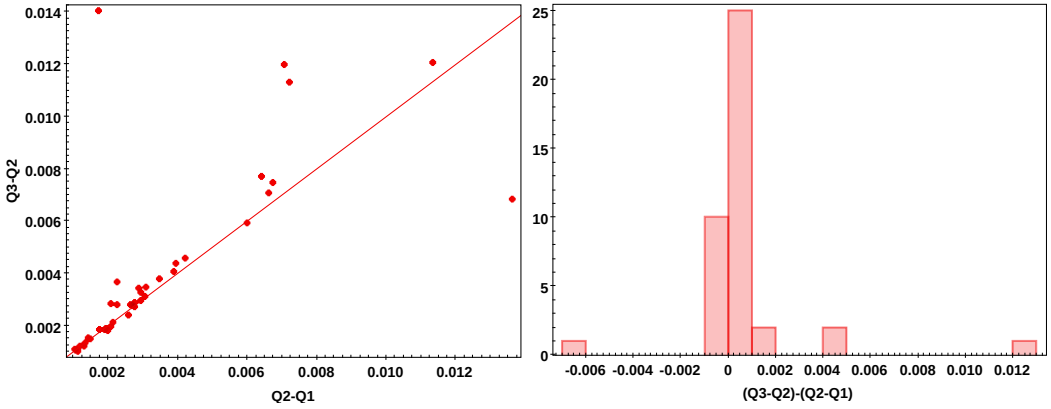

Figure 4. Quartile values for the areas. Median (Q_2), upper (Q_3) and lower (Q_1) quartiles. The one-to-one relation is shown for reference (**left** panel).

In addition, for each area, the χ^2 minimization algorithm (minimize with the lmfit package) calculates the standard deviation (SD). In the lmfit package, the standard deviation of parameters (parameter errors) is calculated based on the covariance matrix, which is obtained after the minimization procedure. The covariance matrix is the result of a linear approximation method and contains information about how the model parameters change relative to each other.

At five areas, SD could not be calculated. Sometimes the minimization method fails to calculate the standard deviations of the parameters due to poor conditioning of the covariance matrix, incorrect initial values, insufficient data, or high noise. We associate these problems with poor data quality. In these cases, we adopted a value of 0.08 mag as SD, slightly higher than the maximum of the calculated values.

As can be seen from Figure 5, in most areas, IQR values were comparable to SD. Therefore, for all areas, the error of the obtained value A_{gal} was assumed to be equal to

$$\sigma = \sqrt{SD^2 + (IQR/2)^2}. \quad (5)$$

It is the value that is used hereafter for comparison with data from other authors.

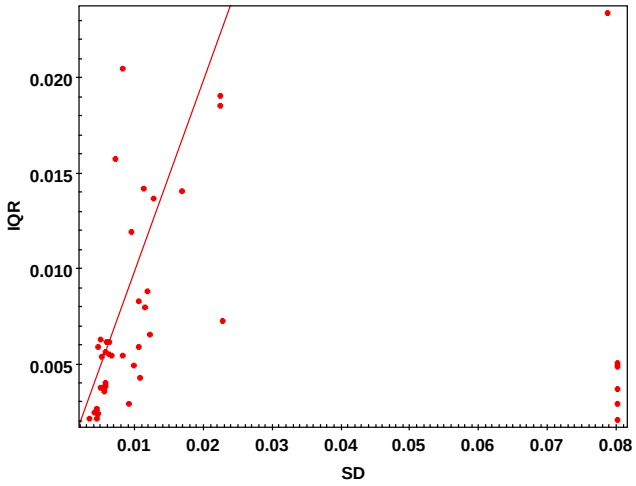

Figure 5. Standard deviation SD and interquartile range IQR for the areas. The one-to-one relation is shown for reference.

3. Comparison of A_{gal} with Other Maps

3.1. Area Centres

First of all, it should be noted that the stars are not uniformly distributed in the test areas. The mean coordinates of all the stars of the area (the "centers of gravity" of the areas) are slightly different from the coordinates of the SN (i.e., the geometric centers of the areas). Figure 6 shows the difference of these coordinates for all areas, as well as the number of stars in the areas. It can be seen that, as expected, the coordinate difference decreases as the number of stars increases. But even in the most "sparsely populated" sites, the "centers of gravity" is usually no further than 0.8 degrees from the geometric center. We believe that for such high latitudes, this is too insignificant a value to noticeably affect the resulting A_{gal}.

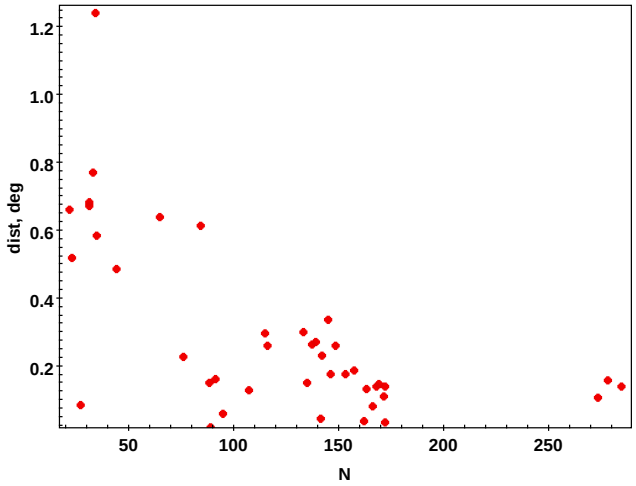

Figure 6. Difference between the mean coordinates of all stars of the area and the coordinates of SN, in degrees vs. the number of stars in the area. See text for details.

3.2. 2D Maps of Galactic Extinction

The A_{gal} values obtained in the previous paragraph can be compared with the A_x values taken from Table 1 of the paper [24], since these latter cases (as seen in Figure 7) are taken, with a few exceptions, from SFD98 [20].

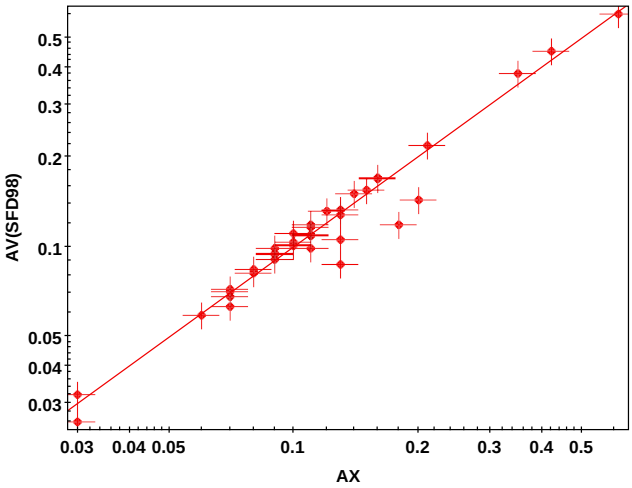

Figure 7. A_x ([24], Table 1) vs. A_V ([20]). According to [24], uncertainty of 10% is assumed. The one-to-one relation is shown for reference.

The results of comparing A_{gal} and A_x [24] are shown in Figure 8. It can be seen that good agreement is achieved for most of the areas.

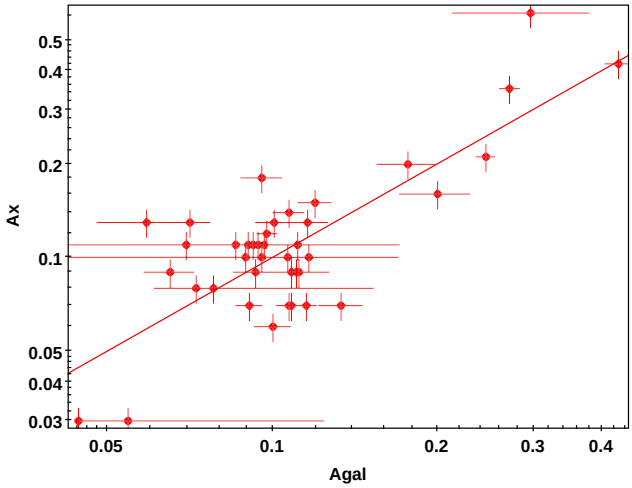

Figure 8. A_{gal} vs. A_x [24]. The one-to-one relation is shown for reference.

However, a comparison of A_{gal} with the more recent map $A(SF11)$ [21] (Figure 9) shows that the values of A_{gal} are systematically overestimated. The values of A_V(SF11) have decreased linearly compared to A_{gal} (and hence to A_x [24] and A_V(SFD98)). It can be roughly estimated that, on average, for the areas studied, A_V(SF11) = 0.8 A_V(SFD98). It can be estimated that the value of the distance to an extragalactic object increases by 3% when the absorption decreases by $0.^m06$.

The difference in results between Schlafly et al. [21,30] and Schlegel et al. [20] arises primarily from the reddening law used and calibration issues in the SFD map. Specifically, Schlafly et al. [21,30] applied a Fitzpatrick reddening law with $R_V = 3.1$ [31], which better fits their measurements, while the SFD98 map overestimates reddening, using O'Donnell [32] reddening law. They found that the SFD98 overpredicts reddening by factors of 1.4 in u-g, 1.0 in g-r, 1.2 in r-i, and 1.4 in i-z, likely due to the less precise reddening law. Moreover,

temperature correction issues also contribute to the inconsistencies, leading to an observed 15% normalization difference between the galactic north and south, attributed to dust temperature errors.

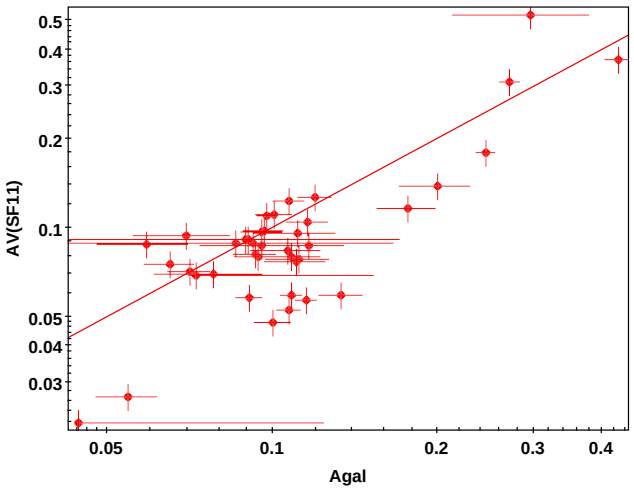

Figure 9. A_{gal} vs. $A(SF11)$ [21]. The one-to-one relation is shown for reference.

3.3. STILISM Service

Figure 10 shows a comparison of our results with data from the STILISM [9]. It should be noted that STILISM provides a 3D-map of interstellar extinction (i.e., the distance dependence of reddening $E_{B-V}(d)$ in different directions up to fixed distances). One would therefore expect that the STILISM values would not exceed the A_{gal} values. Within observational errors, this is the case.

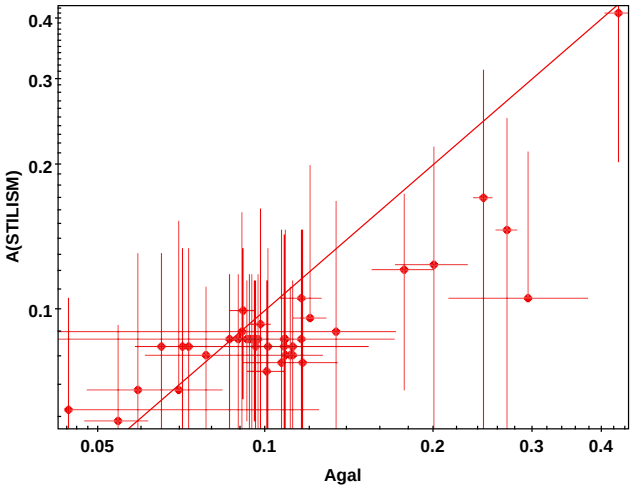

Figure 10. A_{gal} vs. $A(STILISM)$ [9]. The one-to-one relation is shown for reference.

3.4. G23 Map

Finally, we compared our results with the recently published G23 map [7] (see Figure 11). For most areas, the values of $A(G23)$ exceed the values of A_{gal} by $0.^m1$, which implies a 5% decrease in the value of distance to the extragalactic object estimation.

Note that the value of galactic extinction according to G23 can reach several magnitudes at mid-latitudes, despite the fact that the limiting distance does not exceed 2 kpc (see Figure 12).

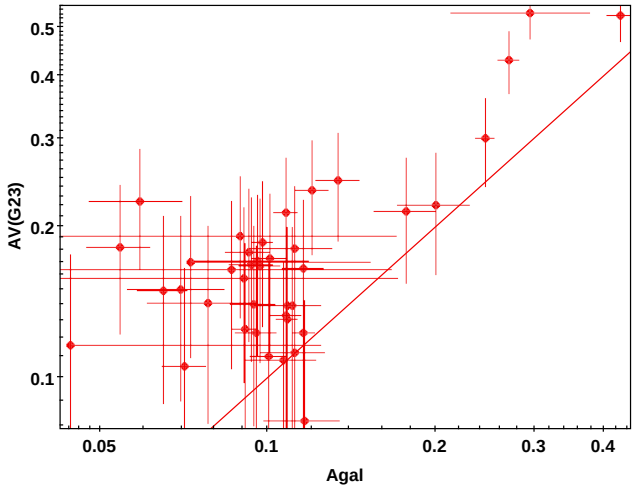

Figure 11. A_{gal} vs. $A(G23)$ [7]. According to Gontcharov (private communication), uncertainty of $0.^m06$ for $A(G23)$ is assumed. The one-to-one relation is shown for reference.

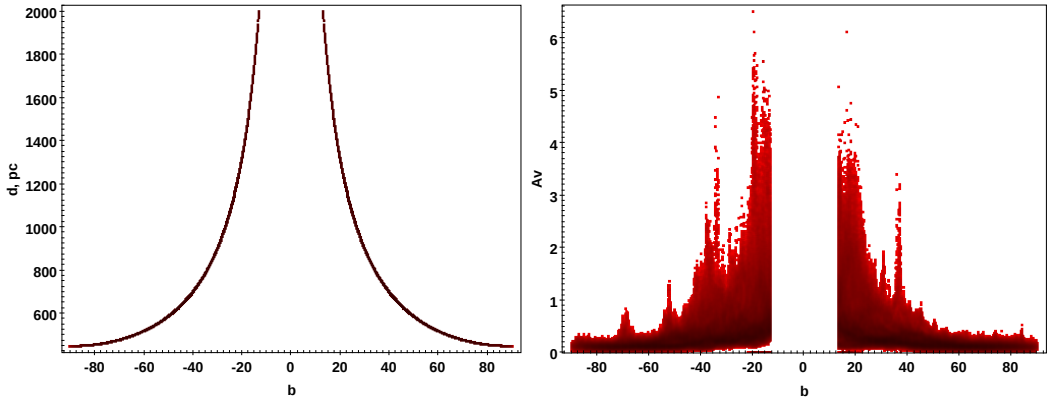

Figure 12. Limiting distance d, pc (**left**) and galactic extinction A_V, mag (**right**) as functions of galactic latitude b in G23 [7].

4. Conclusions

We estimated the galactic extinction value for 42 areas of the northern celestial hemisphere with high galactic latitude (SNe from [24]). Our estimations are based on stellar distances and reddening, inferred from Gaia parallaxes and photometry, and LAMOST atmospheric parameters. We chose this set because [24] is the now classic work that allowed the establishment of the accelerated expansion of the universe. This fact was subsequently confirmed by more abundant and accurate [33–35] data, and we may use these data in the future to further refine our procedure. We should report that our estimates agree well, within observation errors, with those of [24] and [20] (SFD98).

Comparison with other maps shows systematic differences that can cause the distance to the extragalactic object to change by ±3–5%. Apparently, in order to be able to rely on these dust distributions, it is necessary to extend the maps beyond the current limits of a few kiloparsecs, particularly in the inner galaxy. One way of achieving this will be the incorporation of deeper near-infrared photometry, allowing us to see stars through far greater dust column densities.

Author Contributions: The authors made equal contribution to this work; original draft prepared by O.M. All authors have read and agreed to the published version of the manuscript.

Funding: This research was funded by the Ministry of Science and Higher Education of the Russian Federation, according to the research project 13.2251.21.0177 (075-15-2022-1228).

Data Availability Statement: The data presented in this study are available on request from the corresponding author.

Acknowledgments: We warmly thank James Wicker for his great help in preparing the manuscript. The authors thank Maria Pruzhinskaya, Kefeng Tan, and Jingkun Zhao for the valuable remarks and suggestions. We also thank our reviewers, whose constructive comments helped us significantly improve the paper. This research has made use of NASA's Astrophysics Data System, of the SIMBAD database, operated at CDS (Strasbourg, France), of TOPCAT, an interactive graphical viewer and editor for tabular data [36]. The acknowledgements were compiled using the Astronomy Acknowledgement Generator.

Conflicts of Interest: The authors declare no conflicts of interest.

References

1. Parenago, P.P. On interstellar extinction of light. *Astron. Zh.* **1940**, *13*, 3.
2. Fitzgerald, M.P. The Distribution of Interstellar Reddening Material. *Astron. J.* **1968**, *73*, 983. [CrossRef]
3. Neckel, T.; Klare, G. The spatial distribution of the interstellar extinction. *Astron. Astrophys. Suppl. Ser.* **1980**, *42*, 251.
4. Pandey, A.K.; Mahra, H.S. Interstellar extinction and Galactic structure. *Mon. Not. R. Astron. Soc.* **1987**, *226*, 635–643. [CrossRef]
5. Arenou, F.; Grenon, M.; Gomez, A. A tridimensional model of the galactic interstellar extinction. *Astron. Astrophys.* **1992**, *258*, 104–111.
6. Gontcharov, G.A. Influence of the Gould belt on interstellar extinction. *Astron. Lett.* **2009**, *35*, 780–790. [CrossRef]
7. Gontcharov, G.A.; Marchuk, A.A.; Khovrichev, M.Y.; Mosenkov, A.V.; Savchenko, S.S.; Il'in, V.B.; Poliakov, D.M.; Smirnov, A.A. New Interstellar Extinction Maps Based on Gaia and Other Sky Surveys. *Astron. Lett.* **2023**, *49*, 673–696. [CrossRef]
8. Sale, S.E.; Drew, J.E.; Barentsen, G.; Farnhill, H.J.; Raddi, R.; Barlow, M.J.; Eislöffel, J.; Vink, J.S.; Rodríguez-Gil, P.; Wright, N.J. A 3D extinction map of the northern Galactic plane based on IPHAS photometry. *Mon. Not. R. Astron. Soc.* **2014**, *443*, 2907–2922. [CrossRef]
9. Lallement, R.; Capitanio, L.; Ruiz-Dern, L.; Danielski, C.; Babusiaux, C.; Vergely, L.; Elyajouri, M.; Arenou, F.; Leclerc, N. Three-dimensional maps of interstellar dust in the Local Arm: Using Gaia, 2MASS, and APOGEE-DR14. *Astron. Astrophys.* **2018**, *616*, A132. [CrossRef]
10. Green, G.M.; Schlafly, E.; Zucker, C.; Speagle, J.S.; Finkbeiner, D. A 3D Dust Map Based on Gaia, Pan-STARRS 1, and 2MASS. *Astrophys. J.* **2019**, *887*, 93. [CrossRef]
11. Chen, B.Q.; Huang, Y.; Yuan, H.B.; Wang, C.; Fan, D.W.; Xiang, M.S.; Zhang, H.W.; Tian, Z.J.; Liu, X.W. Three-dimensional interstellar dust reddening maps of the Galactic plane. *Mon. Not. R. Astron. Soc.* **2019**, *483*, 4277–4289. [CrossRef]
12. Leike, R.H.; Glatzle, M.; Enßlin, T.A. Resolving nearby dust clouds. *Astron. Astrophys.* **2020**, *639*, A138. [CrossRef]
13. Nekrasov, A.; Grishin, K.; Kovaleva, D.; Malkov, O. Approximate analytical description of the high latitude extinction. *Eur. Phys. J. Spec. Top.* **2021**, *230*, 2193–2205. [CrossRef]
14. Brown, A.G.A. et al. [Gaia Collaboration] Gaia Early Data Release 3. Summary of the contents and survey properties. *Astron. Astrophys.* **2021**, *649*, A1. [CrossRef]
15. Luo, A.L.; Zhao, Y.H.; Zhao, G.; Deng, L.C.; Liu, X.W.; Jing, Y.P.; Wang, G.; Zhang, H.T.; Shi, J.R.; Cui, X.Q.; et al. The first data release (DR1) of the LAMOST regular survey. *Res. Astron. Astrophys.* **2015**, *15*, 1095. [CrossRef]
16. Luo, A.L.; Zhao, Y.H.; Zhao, G. VizieR Online Data Catalog: LAMOST DR5 catalogs (Luo+, 2019). In *VizieR Online Data Catalog*; NASA: Washington, DC, USA, 2019; p. V-164.
17. Avdeeva, A.; Kovaleva, D.; Malkov, O.; Nekrasov, A. Fitting procedure for estimating interstellar extinction at high galactic latitudes. *Open Astron.* **2021**, *30*, 168–175. [CrossRef]
18. Steinmetz, M. et al. [RAVE Collaboration] The Sixth Data Release of the Radial Velocity Experiment (RAVE). II. Stellar Atmospheric Parameters, Chemical Abundances, and Distances. *Astron. J.* **2020**, *160*, 83. [CrossRef]
19. Burstein, D.; Heiles, C. Reddenings derived from H I and galaxy counts: Accuracy and maps. *Astron. J.* **1982**, *87*, 1165–1189. [CrossRef]
20. Schlegel, D.J.; Finkbeiner, D.P.; Davis, M. Maps of Dust Infrared Emission for Use in Estimation of Reddening and Cosmic Microwave Background Radiation Foregrounds. *Astrophys. J.* **1998**, *500*, 525–553. [CrossRef]
21. Schlafly, E.F.; Finkbeiner, D.P. Measuring Reddening with Sloan Digital Sky Survey Stellar Spectra and Recalibrating SFD. *Astrophys. J.* **2011**, *737*, 103. [CrossRef]
22. Vallenari, A. et al. [Gaia Collaboration] Gaia Data Release 3. Summary of the content and survey properties. *Astron. Astrophys.* **2023**, *674*, A1. [CrossRef]
23. Bailer-Jones, C.A.L.; Rybizki, J.; Fouesneau, M.; Mantelet, G.; Andrae, R. Estimating Distance from Parallaxes. IV. Distances to 1.33 Billion Stars in Gaia Data Release 2. *Astron. J.* **2018**, *156*, 58. [CrossRef]
24. Perlmutter, S.; Aldering, G.; Goldhaber, G.; Knop, R.A.; Nugent, P.; Castro, P.G.; Deustua, S.; Fabbro, S.; Goobar, A.; Groom, D.E.; et al. Measurements of Ω and Λ from 42 High-Redshift Supernovae. *Astrophys. J.* **1999**, *517*, 565–586. [CrossRef]

25. Bono, G.; Iannicola, G.; Braga, V.F.; Ferraro, I.; Stetson, P.B.; Magurno, D.; Matsunaga, N.; Beaton, R.L.; Buonanno, R.; Chaboyer, B.; et al. On a New Method to Estimate the Distance, Reddening, and Metallicity of RR Lyrae Stars Using Optical/Near-infrared (B, V, I, J, H, K) Mean Magnitudes: ω Centauri as a First Test Case. *Astrophys. J.* **2019**, *870*, 115. [CrossRef]
26. Cardelli, J.A.; Clayton, G.C.; Mathis, J.S. The Relationship between Infrared, Optical, and Ultraviolet Extinction. *Astrophys. J.* **1989**, *345*, 245. [CrossRef]
27. Jordi, C.; Gebran, M.; Carrasco, J.M.; de Bruijne, J.; Voss, H.; Fabricius, C.; Knude, J.; Vallenari, A.; Kohley, R.; Mora, A. Gaia broad band photometry. *Astron. Astrophys.* **2010**, *523*, A48. [CrossRef]
28. Pecaut, M.J.; Mamajek, E.E. Intrinsic Colors, Temperatures, and Bolometric Corrections of Pre-main-sequence Stars. *Astrophys. J. Suppl. Ser.* **2013**, *208*, 9. [CrossRef]
29. Newville, M.; Stensitzki, T.; Allen, D.B.; Ingargiola, A. *LMFIT: Non-Linear Least-Square Minimization and Curve-Fitting for Python*; Zenodo: Geneve, Switzerland, 2014. [CrossRef]
30. Schlafly, E.F.; Finkbeiner, D.P.; Schlegel, D.J.; Jurić, M.; Ivezić, Ž.; Gibson, R.R.; Knapp, G.R.; Weaver, B.A. The Blue Tip of the Stellar Locus: Measuring Reddening with the Sloan Digital Sky Survey. *Astrophys. J.* **2010**, *725*, 1175–1191. [CrossRef]
31. Fitzpatrick, E.L. Correcting for the Effects of Interstellar Extinction. *Publ. Astron. Soc. Pac.* **1999**, *111*, 63–75. [CrossRef]
32. O'Donnell, J.E. R v-dependent Optical and Near-Ultraviolet Extinction. *Astrophys. J.* **1994**, *422*, 158. [CrossRef]
33. Betoule, M.; Kessler, R.; Guy, J.; Mosher, J.; Hardin, D.; Biswas, R.; Astier, P.; El-Hage, P.; Konig, M.; Kuhlmann, S.; et al. Improved cosmological constraints from a joint analysis of the SDSS-II and SNLS supernova samples. *Astron. Astrophys.* **2014**, *568*, A22. [CrossRef]
34. Scolnic, D.M.; Jones, D.O.; Rest, A.; Pan, Y.C.; Chornock, R.; Foley, R.J.; Huber, M.E.; Kessler, R.; Narayan, G.; Riess, A.G.; et al. The Complete Light-curve Sample of Spectroscopically Confirmed SNe Ia from Pan-STARRS1 and Cosmological Constraints from the Combined Pantheon Sample. *Astrophys. J.* **2018**, *859*, 101. [CrossRef]
35. Brout, D.; Scolnic, D.; Popovic, B.; Riess, A.G.; Carr, A.; Zuntz, J.; Kessler, R.; Davis, T.M.; Hinton, S.; Jones, D.; et al. The Pantheon+ Analysis: Cosmological Constraints. *Astrophys. J.* **2022**, *938*, 110. [CrossRef]
36. Taylor, M.B. TOPCAT STIL: Starlink Table/VOTable Processing Software. In *Astronomical Society of the Pacific Conference Series, Proceedings of the Astronomical Data Analysis Software and Systems XIV, Pasadena, CA, USA, 24–27 October 2004*; Shopbell, P., Britton, M., Ebert, R., Eds.; Astronomical Society of the Pacific: San Francisco, CA, USA, 2005; Volume 347, p. 29.